Editorial Manager(tm) for Bulletin of Earthquake Engineering
Manuscript Draft

Manuscript Number:

Title: Site Effect Variability of the Roio Basin in the Near-Source Area of the L'Aquila Mainshock.

Article Type: SI: 2010 L'Aquila Earthquake

Keywords: L'Aquila earthquake; site effects; strong motion; microtremors; spectral ratios

Corresponding Author: Etienne Bertrand, Ph.D.

Corresponding Author's Institution: CETE Méditerranée

First Author: Etienne Bertrand, Ph.D.

Order of Authors: Etienne Bertrand, Ph.D.;A.-M. Duval;J. Régnier;R.M. Azzara;F. Bergamashi;P. Bordoni;F. Cara;G. Cultrera;G. Di Giulio;G. Milana;J. Salichon

Article Type :

SI: 2010 L'Aquila Earthquake

Title :

Site effect variability of the Roio basin in the near-source area of the L'Aquila mainshock.

Short Title :

Site effects of the Roio basin, L'Aquila

Authors :

E. Bertrand, A.-M. Duval, J. Régnier

CETE Méditerranée - LRPC de Nice, Nice, France

R.M. Azzara, F. Bergamashi, P. Bordoni, F. Cara, G. Cultrera, G. Di Giulio & G. Milana

Istituto Nazionale di Geofisica e Vulcanologia, Italy

J. Salichon

OCA, UMR Géoazur, Sophia-Antipolis, France

Corresponding author :

D. Etienne Bertrand
CETE Méditerranée - LRPC de Nice
56 Boulevard Stalingrad
06359 Nice cedex 4
FRANCE
tel : +33 492 008 161
fax : +33 492 008 139
mail : etienne.bertrand@developpement-durable.gouv.fr

ABSTRACT:

In the frame of the microzonation studies of the April 6th, 2009 L'Aquila earthquake near-source area, we observed local seismic amplifications in the Roio area, a plain separated from L'Aquila city center by mount Luco. Six portable, digital instruments were deployed across the plain from the 15th of April until mid-May 2009. This array recorded up to 152 aftershocks. We analysed the ground motion from these events to determine relative site amplification within the plain and on the surrounding ridges. Horizontal over Vertical spectral ratio on noise data (HVSRN) and on aftershock recordings (HVEQ) as well as standard spectral ratio (SSR) show amplifications at 1.3 Hz and 4.0 Hz on the quaternary deposits. Seismic amplifications in the frequency range between 4 and 6 Hz were also observed on a carbonate ridge of Colle di Roio located on the northwest border of the plateau. A small amplification has also been noticed close to the top of mount Luco, another rocky site. This paper details the results we have obtained and addresses their interpretation.

Keywords: L'Aquila earthquake; site effects; strong motion; microtremors; spectral ratios

1 INTRODUCTION

The epicentral region of the 2009 L'Aquila earthquake (central Italy) suffered from severe damage, but the distribution of this damage was not homogenous over the area. If the construction's vulnerability can explain part of this feature, it may also be linked to the variability of the strong ground motion due to local site effects. It is well known that these site effects are strongly influenced by the lithological features of the superficial structures, which may induce resonance phenomena as well as by the topography of the surface and layers interfaces, which may induce focusing effects. The soil's fundamental resonance frequency can be evaluated on the field, thanks to various methods. Experimental methods are commonly based on the recording of surface vibration due to earthquake or ambient noise. In the case of earthquake data, the recordings on a soil site are often compared to the ones at a rocky station by computing spectral ratios (Duval, 1996). The site effects are also commonly evaluated using Horizontal over Vertical spectral ratios at only one station (e.g. Lermo and Chavez-Garcia, 1993; Field and Jacob, 1995; Theoulidis and Bard, 1995). The ambient noise data is used to compute H/V spectral ratios according to Nakamura's procedure (Nakamura, 1989).

To better estimate the strong ground motion during the 2009 L'Aquila main shock in the epicentral area, we took part in the setting up of temporary seismological arrays in the region. The stations have been installed nearby or inside the most damaged centers, where the macroseismic intensity reached the IX/X MCS degree (Galli et al., 2009) and where coseismic surface effects have been observed (Emergeo Working Group, 2010). This paper deals with the experiment we conducted in the Roio plain, a rural quarter west of L'Aquila town and composed of ancient villages located right above the hypocenter, where the damage distribution was not homogenous (Fig. 1). The seismic stations have

been equipped with velocimeters (Lennartz Le3d-5s) and/or accelerometers (Geosig AC23) coupled with Ageocodagis Kephren digitizers. In most of the cases, the energy has been supplied to the station by means of solar panels and the time accuracy is guaranteed by GPS antenna connection. The accelerometric and velocimetric seismic stations have been installed outside the buildings (Fig. 2). In particular, the accelerometric sensors recorded the larger aftershocks to evaluate the possible presence of non-linear effects. The site effects are investigated by computing ratio of the Fourier spectrum of the horizontal components over the vertical one of ambient vibration recordings as well as on the aftershocks data. We compare these ratio to the one deduced from the classical standard spectrum ratio (SSR). The sensitivity of the SSR is then analyzed according to the epicentral distance, the ground motion strength and the reference station-source azimuth.

Figures 1 and 2

2 GEOLOGICAL SETTING

The earthquake sequence of 2009 happened in the central Apennines, in an extensional tectonic regime context with prevalent SW-NE direction that has been shaping the region since the mid-Pliocene (Pace et al., 2006). This tectonic regime is in particular at the origin of NW-SE oriented basin aperture such as the Aterno River Valley. The deposits filling the valley are dated from the Middle Pleistocene to present and are formed by alternations of calcareous silt, gravel and conglomerate layers. Coarse debris deposits heterogeneously covert he top of the soil column.

The study area is located in the western sector of the Aterno valley and is characterized by the outcropping of a thick carbonate succession belonging to the Latium-Abruzzi Neritic Domain (Centamore et al., 2002; Boccaletti et al., 1990; Cipolari and Cosentino, 1995; Brachi et al., 1998; Centamore and Rossi, 2009). The present morphostructural pattern reflects the effects of a polyphase tectonic activity developed since Trias to Present. In particular, starting from the upper part of the Lower Messinian, the area was involved in the late compressive phase, during which thrust and associated minor structures (such as folds, splays, tear faults and cataclastic zones) developed.

The Roio plain is a semi-graben depression bordered by carbonate reliefs and filled by Upper Pliocene - Lower Pleistocene continental deposits. (Fig. 3) The development of the Roio basin was controlled by several factors, such as a first Messinian compressional phase accompanied by a regional uplift, and post-orogenic (Middle Pliocene to Lower Pleistocene) extensional tectonics which favoured the deepening of an asymmetric graben delimited by a west-dipping Apennine extensional fault system on the eastern side and by an anticline on the northern side.

According to the first results of the geotechnical data gathering conducted in the frame of the Roio area seismic microzonation ordered by the Italian civil protection (http://www.protezionecivile.it/cms/view.php?dir_pk=395&cms_pk=17329), the middle of the plain is filled with a mix of clay, clayey silt, alluvium and colluvium characterized by an increasing consistency with increasing depth. Locally, a sandy layer reaching a thickness up to 18 meters overlies the clayey silt layer. The maximum thickness of these deposits is supposed to reach at least 60 meters in the center of the plain and 15 meters on the border (Fig 4).

The plain is separated from the Aterno valley by several carbonate ridges such as the Colle di Roio one, in the North-western corner of the map on figure 3, which reaches an altitude of 800 meters a.s.l. At Colle di Roio, the ridge is characterized by the overthrust of the Mesozoic carbonatic deposits above a Miocenic clay-marls succession, with the development of a N130° trending asymmetric anticline (Fig.4) (Hailemikael *et al.*, 2010). An equivalent structure should be found under the University of L'Aquila, above Poggio di Roio.

Figures 3 and 4

3 DESCRIPTION OF THE EXPERIMENT

Six seismological stations were set up in the Roio area during one month, starting from the 15th of April, recording up to 126 aftershocks with magnitudes ranging from 1.4 to 4.4 at epicentral distances smaller than 26 km (Fig. 5). The position of the stations in regards to the local geology is given in Figures 3. and 4. Four stations were installed on the carbonated ridge bordering the plain to the North. Located in Colle di Roio, FRR4 is composed of a single Le3D5s velocimetric seismometer. In Poggio di Roio, we installed two stations: FRR2 (Fig. 2), in a heavily damaged area supplied with a single Geosig AC23 accelerometer, whereas FRR3 is located in an area where almost no damage was observed. This latter station was equipped with an accelerometer as well as a velocimeter both coupled to the same acquisition system. In order to detect any topographical effects that could explain the damage to the buildings of L'Aquila Engineering University overhanging Poggio di Roio, we installed both an Le3D5s and an AC23 sensor at FRR1 site, located almost at the top of the mountain. The two last instrumented sites are located in the plain. At FRR5, in the severely damage Roio Piano village, we put an accelerometer and a velocimeter, whereas in Santa Rufina (FRR6) a single accelerometer was set up.

Figure 5

4 SEISMIC NOISE RECORDINGS ANALYSIS

The method based on microtremor for estimating dynamic characteristics of surface layers, was first introduced in Japan in early 1970 (Nogoshi and Igarashi, 1971). After the paper by Nakamura (Nakamura, 1989), many people paid a renewed attention to this technique of estimating dynamic ground characteristics, since clear and reliable information was provided by very simple and inexpensive noise measurements. In recent years, the theoretical background of the method has been studied (e.g. SESAME project, 2004) and there have been many successful experimental studies based on this method.

The principle of the method consists of recording the ambient vibrations according to 3 directions (a vertical, and two horizontals). Signals are processed numerically to obtain the corresponding Fourier spectra. The horizontal spectra are then divided by the spectrum of the vertical component. This ratio (HVNSR) computation results in a curve that presents a peak corresponding to the site's fundamental resonance frequency. It is assumed to be the frequency below which there is no amplification of the surface ground movement during seismic solicitation.

Since accelerometers are not able to record ambient vibrations due to their low sensibility, the HVNSR has been only computed at site equipped with Le3D5s velocimeters (FRR1, FRR3, FRR4 and FRR5). The data has been processed using the SESARRAY software developed in the frame of the SESAME European project (Wathelet, 2005). The FFT have been computed considering several 60 second long windows of stationary signal, allowing us to compute the HVNSR down to 0.2 Hz, in good agreement with the frequency band of the Le3D5s seismometer. Their selections are completed using the ratio computation of the short-term-average (STA) over the long-term-average (LTA). Usually, noise signal is considered to be stationary when this ratio lies between 0.3 and 2. The spectrum smoothing is done with the Konno and Ohmachi (1998) smoothing technique. This method is recommended by SESAME guidelines (SEASME, 2004), as it accounts for the different number of points at low frequencies.

Figure 6 presents the HVNSR curves derived from the ambient vibration recordings in the Roio plain. According to the SESAME criteria, FRR3 station in Poggio di Roio exhibits a flat HVNSR curve between 0.2 Hz and 10 Hz. On the contrary, the curves obtained at stations FRR1, FRR4 and FRR5 show amplifications at 2.6 Hz, 5.0 Hz and 4.2 Hz respectively. Thus, FRR3 seems to be the best candidate for the reference site (LeBrun, 1997, LeBrun *et al*., 2001). Nevertheless, the HVNSR for this station shows value between 2 and 3 for frequencies between 2 and 4 Hz that could have a small impact in the SSR results. Indeed, we might slightly underestimate the seismic site responses at these frequencies.

Figure 6

The HVNSR method is based on the hypothesis of sedimentary plane layers and the ratio should be more or less equivalent no matter the orientation of the horizontal component considered. To assess this statement, we computed the HVNSR after rotation the horizontal component between 0° and 180°. The results we obtained are shown in figure 7 for station FRR1, FRR4 and FRR5. If at FRR5 the result doesn't seem to depend on the observation direction considered, at FRR4 and FRR1 the ratio varies significantly with the azimuth. Indeed, the maximum ratio observed for FRR1 at 2.6Hz is just obtained for azimuths close to 120°N, and the 5.0 Hz peak at FRR4 is present only for azimuths around 40°N. Therefore, at these stations, a 3D site effect is strongly suspected. This assumption shows a good agreement with the geological setting of the stations (Fig. 4).

Figure 7

5 AFTERSHOCK RECORDINGS ANALYSIS

Two techniques have been applied to the recordings we made in the Roio plain. Following Langston (1979), we first applied the H over V spectral ratio method to the aftershocks recordings (HVEQ) in order to compare the results we obtained from microtremor data. The second method considered (first described in Borcherdt and Gibbs, 1970) consists of computing the site transfer function by a comparison of the gathered data with simultaneous recordings at a reference station placed directly on a flat-outcropped rock. The acquired signals are processed numerically to obtain their Fourier spectrum and the ratio site-over-reference (also called Standard Spectral Ratio, SSR) is then computed. For a given place, these spectral ratios are dependent on the earthquake source. According to Field and Jacob (1995), reliable results are only obtained considering a mean of several spectral ratios computed from a significant number of well-distributed earthquakes over a large magnitude and distance range. When this condition is full-filled, the mean spectral ratio can be considered as an estimated transfer function of the investigated site. The main difficulty of the method lies in the choice of the reference station. The critical assumption made is that the surface rock-site record used as a reference is equivalent to the input motion at the base of the soil layers, excluding the free surface effect (Dubos *et al.*, 2003). However, surface rock-site can have a site response of its own, which could lead to an underestimation of the seismic hazard when these sites are used as reference sites (Steidl et al., 1996). Thus, even if FRR1 and FRR4 are located on a rocky sites according to the geological map (Fig. 4), these stations cannot be considered as references since their HVNSR is not flat (Fig. 5); the choice of FRR3 as a reference site is the most appropriate, as the HVNSR does not exceed values of 2-3 at any frequency. It's also the reason why we equipped this site with a velocimetric sensor as well as an accelerometric one.

From April 15, 2009 to May 14, the stations in Roio plain have recorded 126 aftershocks. The magnitude (Ml) of the recorded aftershocks reached a maximum of 4.4, the epicenter distance (from

the reference station) ranged from 0.9 km to 26 km (Figure 3).
As an example, the NS time series of the April 18 event (Ml=3.8, epicentral distance = 13 km) is presented in figure 8. These recordings clearly point out the seismic movement amplification at almost all stations compared to FRR3. This amplification seems to be the largest at FRR6 and FRR5, while the motion at FRR2 is almost equivalent to the one recorded at the reference station.

Figure 8

A window of about 30 seconds has been considered for almost all of the signals, in order for the analysis to be relevant down to a frequency of 0.3 Hz. Because of the short source-to-site distance, it was impossible to separate the P and S arrivals and both are thus included in the analysis. The spectral ratio is calculated only at frequencies for which the signal-to-noise is larger than 3 for both the reference station and the observed one. To process the signal, the time series are tapered with a cosine taper with a length of 10% of the considered window and a Konno and Ohmachi (1998) smoothing scheme is applied to the results of the FFT. For the SSR, we present the mean ratio for both the horizontal components at each station, plus or minus one standard deviation. For the HVEQ, the horizontal components are first combined and then the Horizontal over Vertical ratio is computed for each earthquake; the results are shown in terms of mean plus or minus one standard deviation curves for each station.

Figure 9 displays the HVEQ compared to the HVNSR at stations FRR1, FRR3, FRR4 and FRR5. We notice a very good agreement between the two types of computations everywhere. More precisely, the shapes of the curves are similar, but the level of amplification found is notably lower for the HVNSR than for the HVEQ. Surprisingly, the mean HVNSR is very close to the 16th percentile curve of the HVEQ over the investigated frequency band at almost all of the stations. But at FRR5 both of the means are equivalent below 1.6 Hz.

Figure 9

SSR were computed using both accelerometric and velocimetric data, when available. In order to compare the results considering the two types of data separately, we plotted the one obtained at station FRR5 on figure 10. Because of their difference of sensibility, the velocimeter recorded significantly more aftershocks than the accelerometric sensor. It is particularly noticeable at low frequencies. Indeed, for frequencies lower than 1 Hz, less than 30 records have a signal-to-noise ratio larger than 3 among the accelerometric database, whereas the number of signals used increases at almost 120 for the velocimetric data. Nevertheless, the curves derived from the accelerometric data are very similar to the one derived from the velocimetric ones, with the exception of the very low frequencies (under 0.4 Hz).

The amplification of both the horizontal components is starting roughly at 2 Hz and it reaches a level of 5.2 at 4.0 Hz on the EW component and 4 at 4.2 Hz on the NS component. Amplification is also seen on the vertical component of the ground motion with a maximum of 3.2 at 8.2 Hz.

Figure 10

Figure 11 show the comparison between HVEQ and SSR mean curves. HVNSR and HVEQ are consistent at each site. (Fig. 9) However, the SSR differs from the Horizontal over Vertical ratios at station FRR2, FRR4 and FRR1, suggesting either a topographical or a 3D effect, as shown by the rotational HVNSR (Fig. 7). In this case, the SSR technique should be considered as more reliable in the estimation of the site response. Nevertheless, it seems that both of the Horizontal over Vertical techniques point out the same resonance frequency as the SSR method. This frequency is equal to 2.6 Hz, 5.0 Hz and 3.0 Hz at FRR1, FRR4 and FRR2 respectively. FRR6 is the site where the strongest seismic amplification has been detected. Indeed, at this station, the maximum reaches 9 at 1.3 Hz for the NS component.

Figure 11

The horizontal ground motion at FRR2 is, on average, twice as strong as the one at FRR3 between 2Hz and 10Hz. These ground motion amplifications, as well as the vulnerability of the construction, are probably the reason why the damage levels surrounding the two stations differed. Indeed, near FRR3 the houses suffered less than the ones located in the vicinity of FRR2.

Not only the sites in the plain exhibit strong seismic ground motion amplification. For instance, FRR1, located near where the Engineering University of L'Aquila stands on the top of a mountain, presents a strong amplification of around 3.6 Hz. This amplification could be related to a topographical effect (Chavez-Garcia *et al.*, 1996, 1997).

At Colle di Roio (FRR4), the rock site shows remarkable seismic amplification effects, explained by Hailemikael *et al*. (2010) by the seismic impedance due to the difference of jointing conditions of two adjacent rock masses that are in contact at a very shallow depth.

In the center of the valley, the resonance frequency varies from 1.3 Hz at FRR6 to 4.0 Hz at FRR5. This frequency discrepancy is in good agreement with the difference of the local geology under the two stations. Indeed, FRR5 is installed on massive clastic deposits with a thickness greater than 25 meters, whereas FFR6 lies on a soil column composed of sand, clay and silt layers with a thickness greater than 50 meters. The difference of alluvium thickness combined with the disparity of the alluvium quality explains the resonance frequency variation between the two sites.

6. STABILITY OF SPECTRAL RATIOS

Previous studies already assessed the stability of the Fourier spectrum ratio (e.g. Yamazaki and Ansary, 1997), most of them concluding that the ratio is stable irrespective of magnitude and event location when a simple plane layered structure exists below the site. Another issue concerns the source proximity from the considered array when using the SSR technique. As a rule, in order to remove the source effect and the regional wave propagation from the source to the basement of the structure that led in the site effects, one is to consider only events occurring at a range of at least 5 times greater than the distance between the observation site and the reference station (Duval, 1994, Dubos, 2003). In order to check if considering the events occurring right beneath the studied zone in the SSR computation distorts the result and to investigate the dependence of the SSR on seismic ground motion strength or on main incoming wave azimuths, we display in figure 12 the variation of the frequency corresponding to the detected ratio maximum, *F(Amax)*, from the individual SSR computed at FRR5, according to the peak ground acceleration recorded (PGA), the site-source azimuth and the epicentral distance at the reference station. On the same figure, we also present the dependence of the fundamental resonance frequency, *Fo*, defined as the frequency corresponding to the first peak detected on the SSR. In this latter case, the peaks greater than 3 are only taken into account. The same work has been done at the other stations but nothing more could be deduced from it.

Figure 12

On figure 12 we first notice that at FRR5 the resonance frequency generally equals *F(Amax)*. Nevertheless, the variability of *F(Amax)* is larger than the one of *Fo* and often the resonance frequency is not the one for which the SSR is maximum, especially for PGA larger than 3.10^{-4} g. It is also remarkable that a few ratios present a *Fo* value near 1.3 Hz, which is close to the resonance frequency observed at FRR6. This observation may suggest that some energy of the trapped wave in the sediments below FRR6 station, which produce the resonance at 1.3 Hz, propagates a little bit further and is able to reach the station FRR5. Furthermore, the variability of *Fo* seems to be lower for distances greater than 19 km, but the number of events recorded at distances larger than 20 km is very small and it is difficult to draw any conclusions here.

Values of F(Amax) exceeding 6Hz are found from recordings of events at a distance of less than 15 km and coming from a given direction (Fig. 12). Plotting the aftershock position in figure 13, we can observe that the events producing a maximum on the SSR curve at frequencies higher than 6.0 Hz are located mainly south-west of the Roio plain. Figure 14 displays the mean SSR computed considering ratios grouped by *F(Max)*, e.g. curves with F(Amax) lower or higher than 6Hz. For both groups the resonance frequency remains the same, whereas the curves differ notably at higher frequencies. Thus it appears that using events occurring directly below the seismological array to estimate this resonance frequency is appropriate, at least considering small to moderate magnitudes.

Figures 13, 14

7 CONCLUSION

The April 6th, 2009 earthquake that struck the Abruzzo region caused hundreds of causalities and mostly affected the city of L'Aquila and the village of the upper and middle Aterno Valley. Many buildings collapsed and the ancient masonry suffered particularly. Local site effects are one of the keys that can explain the damage distribution, along with the distance to the source and the vulnerability of the construction. In order to assess these effects in the Roio plain, we set up 6 seismological stations in the vicinity of the main shock epicenter. The results obtained confirm the presence of large amplification effects. These amplifications have been detected not only at the stations located on alluvium in the plain but also at the ones lying on rocky sites at the edges of the plain. Large discrepancies in the amplification level between the methods have been shown for these stations, but HVNSR, HVEQ and SSR are very similar at the stations located in the plain on quaternary sedimentary deposits. On the rocky hills, the SSR is more reliable than the H-over-V techniques for estimating the transfer function of the site even if the resonance frequency seems to be well recovered by the latter methods. These functions vary strongly from one recording point to the other. For instance, in the Roio plain the fundamental resonance frequency at station FRR5 has been found to be nearly 4.0 Hz, whereas FRR6, at a distance of less than 700 meters, is equal to 1.3 Hz. At these stations, the resonance frequency does not change with distance, azimuth or PGA, but the shape of the transfer function varies according to the considered recordings in the computation of the mean SSR. The seismic ground motion at the instrumented sites was in all likelihood amplified during the main shock in the same frequency range and level shown in our SSR computations. These seismic amplifications certainly participated in the high level of damage observed in the villages of the Roio basin during the April 6th earthquake.

REFERENCES

Barchi MR, Minelli G, Pialli G (1998). The crop03 profile: a synthesis of result on deep structures of the northern apeninnes. Mem. Soc. Geol. It., **52**, 383-400.

Blumetti AM, Di Filippo M, Zaffiro P, Marsan P, Toro B (2002). Seismic hazard of the city of L'Aquila (Abruzzo — Central Italy): new data from geological, morphotectonic and gravity prospecting analysis, *Studi Geologici Camerti* **1**, 7–18.

Boccaletti M, Calamita F, Deianna G, Gelati R, Massari F, Moratti G, Ricci Lucchi F (1990). Migrating foredeep thrust belt system in the Northern Apennines Alps. *Paleogeo. Paleocli. Paleoeco*., **77**, 3-14.

Borcherdt RD, Gibbs JF (1970). Effects of local geological conditions in the San Fransisco Bay region on ground motions and the intensities of the 1906 earthquake. *Bull. Seism. Soc. Am*., **66**, 467-500.

Centamore E, Rossi D (2009). Neogene-Quaternary tectonics and sedimentation in the Central Apennines. *Italian Journal Geosciences*, **128(I)**, 73-88.

Centamore E, Fumanti F, Nisio S (2002). The Central-Northern Apennines geological evolution from triassic to neogene time. *Boll. Soc. Geo. It*., **vol. Spec. 1**, 181-197.

Chavez-Garcia FJ, Rodriguez M, Field EH, Hatzfeld D (1997) Topographic site effects. A comparison of two non reference methods. *Bull. Seism. Soc. Am.*, **87**, 1667-1673.

Chavez-Garcia FJ, Sanchez LR, Hatzfeld D (1996) Topographic site effects and HVSR. A comparison between observation and theory. *Bull. Seism. Soc. Am*., **86**, 1559-1573.

Cipollari P, Cosentino D (1995). Miocene unconformities in Central Apennines: geodynamic significance and sedimentary basin evolution. *Tectonophysics*, **252**, 375-389.

De Luca G, Marcucci S, Milana G, Sanò T (2005). Evidence of Low-Frequency Amplification in the City of L'Aquila, Central Italy, through a Multidisciplinary Approach Including Strong- and Weak-Motion Data, Ambient Noise, and Numerical Modeling. *Bull. Seism. Soc. Am.* **95**: 1469-1481.

Dubos N, Souriau A, Ponsolles C, Fels JF, Sénéchal G (2003). Sites response estimates at the city of, Lourdes, Pyrenees, France, using the spectral ratio method. *Bull. Soc. géol. Fr*., **174, n°1**, 33-44.

Duval AM (1994). Détermination de la réponse d'un site aux séismes à l'aide du bruit de fond : Evaluation experimentale. *PhD Thesis, Univ. Paris 6*, 223p.

Field EH, Jacob KH (1995). A comparison and test of various site-response estimation techniques, including three that are not reference-site dependen. *Bull. Seism. Soc. Am.*, **85**, 1127-1143.

Galli P, Camassi R (eds) (2009). Rapporto sugli effetti del terremoto aquilano del 6 aprile 2009, *Rapporto congiunto DPC-INGV*, 12 pp.

Hailemikael S, Lenti L, Martino S, Paciello A, Scarascia Mugnozza G (2010). 2D numerical modelling of observed amplification effects on a carbonate ridge: the Colle di Roio (Italy) case-history. *Proceedings of the 14th European conference on Earthquake Engineering, 14ECEE,* Ohrid, Macedonia.

Konno K, Ohmachi T (1998). Ground motion characteristics estimated from spectral ratio between horizontal and vertical components of microtremors. *Bull. seism. Soc. Am.*, **88-1**, 228-241.

Lermo J, Chavez-Garcia FJ (1993). Site effect evaluation using spectral ratios with only one station. *Bull. Seism. Soc. Am.*, **83**, 1574-1594.

LeBrun B (1997). Les effets de site: étude expérimentale et simulation de trois configurations. *PhD Thesis, Univ. Grenoble I, France*, 208 p.

LeBrun B, Hatzfeld D, Bard PY (2001). Site effect study in urban area: experimental results in Grenoble (France). *Pure appl. geophys.*, **158**, 2543-2557.

Nakamura Y (1989). A method for dynamic characteristic estimation of subsurface using microtremors on the ground surface. *Quarterly Report*, **Vol. 30 (1)**, RTRI, Japan.

Nogoshi M, Igarashi T (1971). On the amplitude characteristics of microtremor, *Jour. Seism. Soc. Japan*, **23**,264-280.

Pace B, Peruzza L, La vecchia G, Boncio P (2006). Layered seismogenic source model and probabilistic seismic-hazard analyses in central Italy, Bull. Seism. Soc. Am., 96, 107–132, doi: 10.1785/0120040231.

SESAME European project n° EVG1-CT-2000-00026 (2004). Guidelines for the implementation of the H/V spectral ratio technique on ambient vibrations. Report n°D23.12, http://sesame-fp5.obs.ujf-grenoble.fr.

Steidl JH, Tumarkin AG, Archuleta RJ (1996). What is a reference site ?. *Bull. Seism. Soc. Am.*, **86 (6)**, 1733-1748.

Theodulidis NP, Bard PY (1995). Horizontal to vertical spectral ratio and geological conditions: an analysis of strong motion data from Greece and Taiwan (SMART-1). Soil Dynamics and Earthquake Engineering, **14**, 177-197.

Wathelet M (2005). Array recordings of ambient vibrations: surface wave inversion. Ph.D. Thesis, Liège University, May 12, 2005.

Yamazaki F, Ansary MA (1997). Stability of H/V spectrum ratio of earthquake ground motion. *Transaction of the 14th International Conference on Structural Mechanics in Reactor Technology (SMiRT 14), Lyon, France*.

Figure captions

Fig. 1 Temporary seismological stations installed on the Roio plain during the L'Aquila 2009 earthquake sequence.

Fig. 2 Accelerometer at station FRR2 in Poggio di Roio.

Fig. 3 Geological setting of Roio area (after the geological map distributed by the Italian Civil Protection http://www.protezionecivile.it/docs/www.ulpiano11.com/docs/microzonazione_pdf/Macroarea8/M8_Geologica.pdf).

Fig. 4 Geological cross-sections through the Roio plain (after the sections distributed by the Italian Civil Protection http://www.protezionecivile.it/docs/www.ulpiano11.com/docs/microzonazione_pdf/Macroarea8). See Fig. 4 for legend. The position of the seismological stations is approximate.

Fig. 5 Aftershocks recorded by the temporary array set in the Roio plain. Colors are according the PGA at station FRR3.

Fig. 6 HVNSR curves obtained at stations in the Roio plain.

Fig. 7 HVNSR amplitude in function of the azimuth. The horizontal components are first rotated and then the H-over-V ratios are computed using the classical scheme.

Fig. 8 Time histories (N-S and vertical component) of the April 18th, 09:04:56 aftershock (distance = 13 km, M_L=3,8). Acceleration (left) and velocity (right) of the ground motion are shown at the relevant station. Note the difference between amplitude scales for Z and NS plots.

Fig. 9 HVNSR (dashed line) and HVEQ (median: thick ; 16th and 84th percentiles: thin) curves obtained at stations FRR1, FRR3, FRR4 and FRR5.

Fig. 10 Standard spectral ratios (SSR) obtained at station FRR5 considering station FFR3 as a reference (from top to bottom: E-W, N-S and vertical component). On the left, the curves are computed from the accelerometric data and on the right the curves are computed from the velocimetric ones. The dashed curve represents the number of recordings considered for each frequency.

Fig. 11 Comparison between H/V spectral ratio on aftershock (HVEQ) data and standard spectral ratio (SSR).

Fig. 12 Variation of the frequency corresponding to the maximum (*F(Amax)*) and to the first peak (*Fo*) on individual SSR computed for FRR5 according to the PGA at FRR3 (top), epicentral distance at station FRR3 (middle) and azimuth at FRR3 (bottom).

Fig. 13 Distribution of the aftershocks used to compute the SSR at FRR5 (EW component). The triangle color refers to the frequency for which the maximum is detected on the individual SSR.

Fig. 14 Mean SSR considering the curves having *F(Amax)* lower than 6.0 Hz (left) and larger than 6.0 Hz (right).

figure 1

Click here to download high resolution image

figure 2
Click here to download high resolution image

figure 3

Click here to download high resolution image

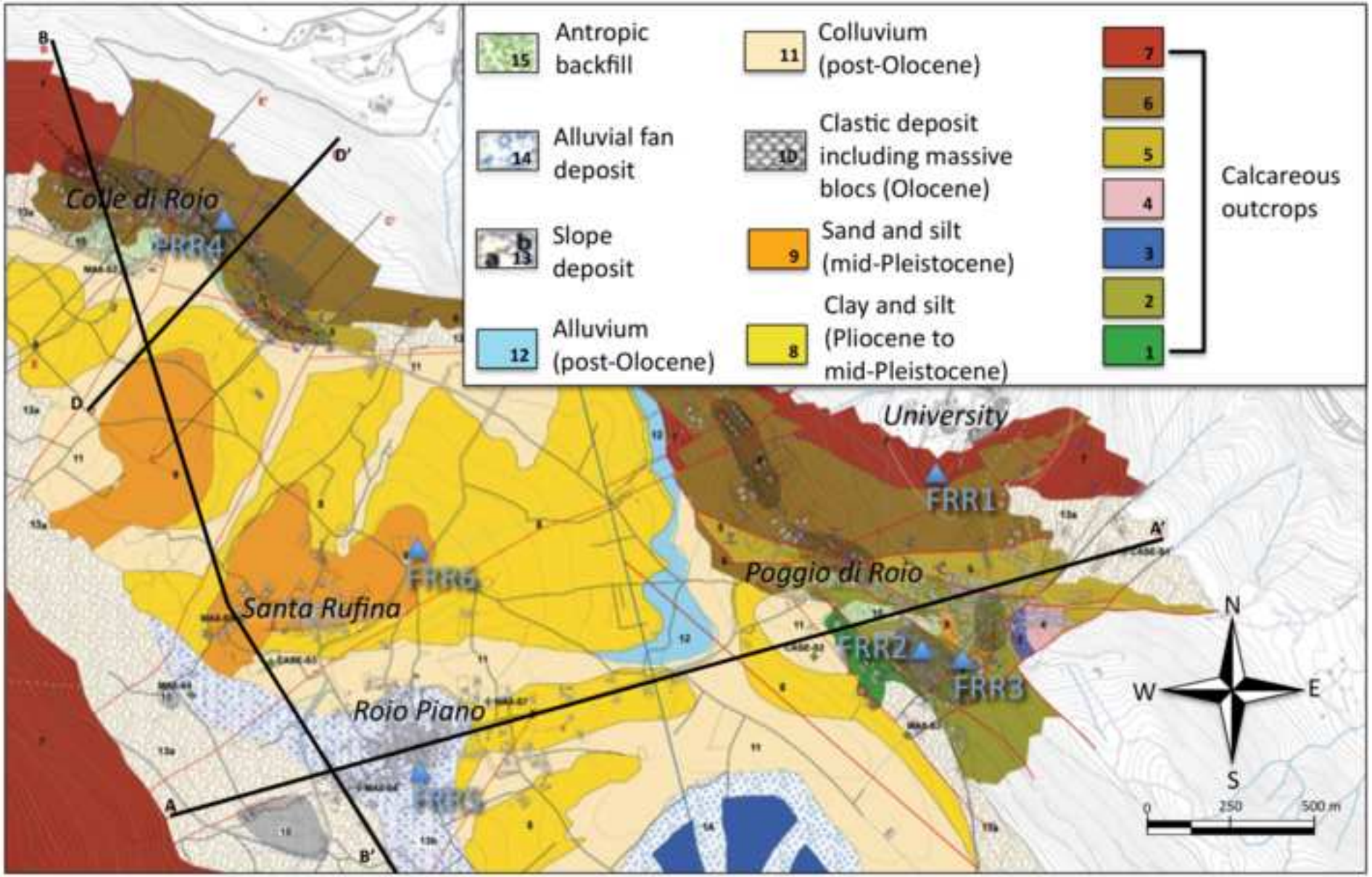

figure 4

Click here to download high resolution image

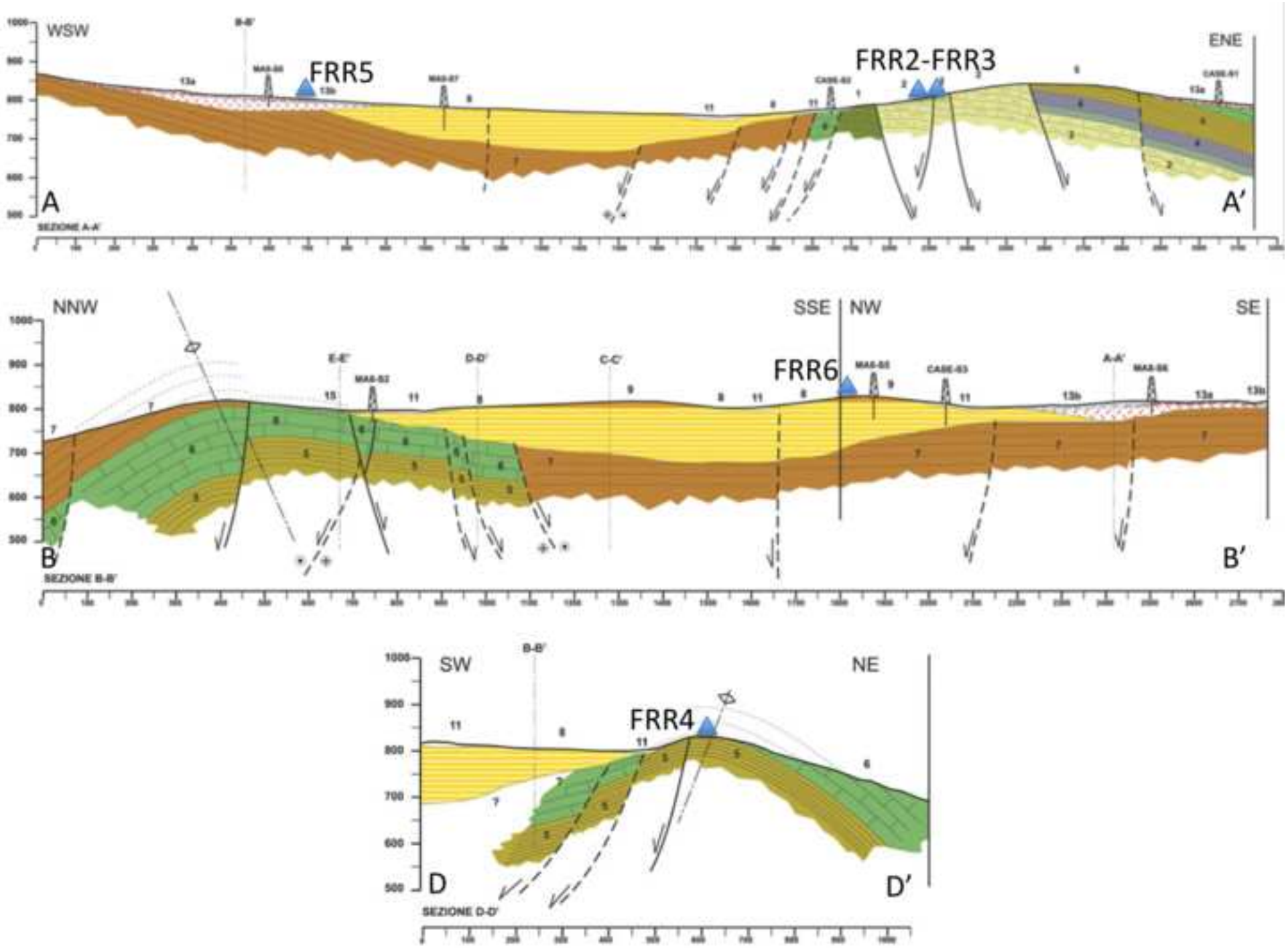

figure 5

Click here to download high resolution image

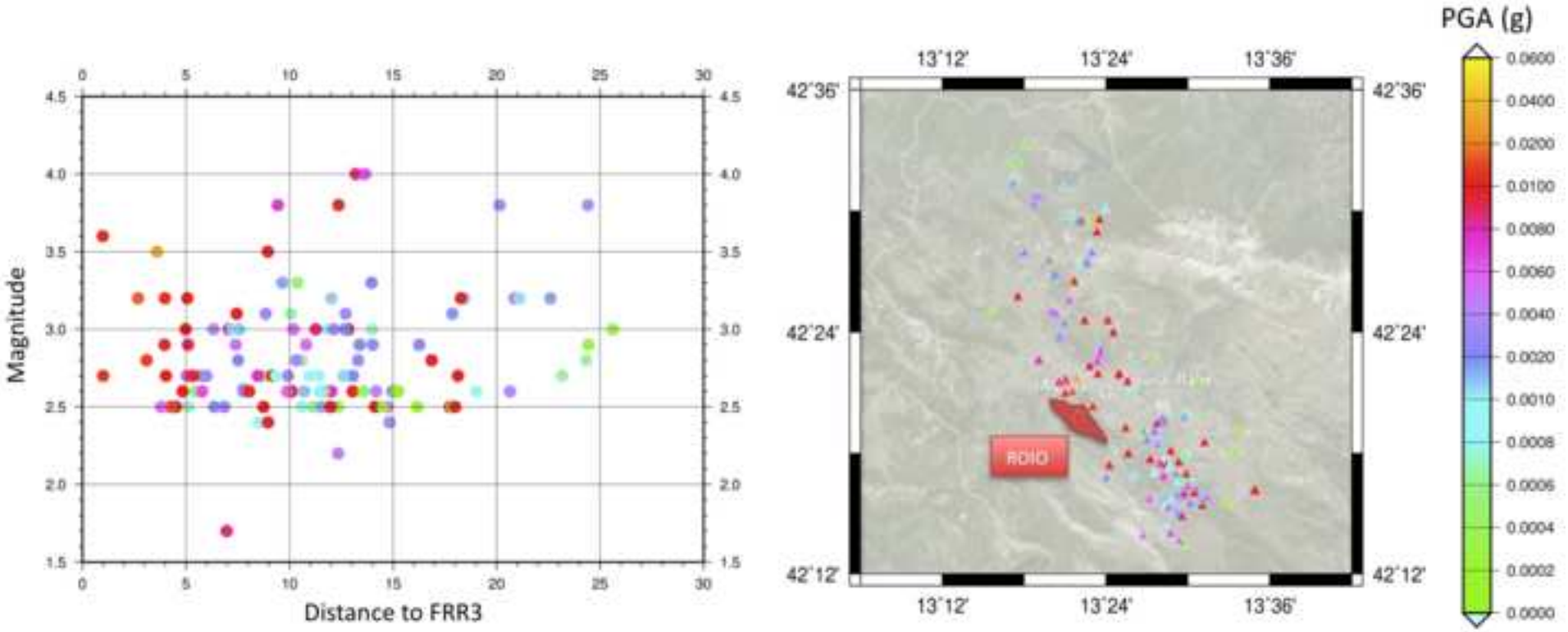

figure 6

Click here to download high resolution image

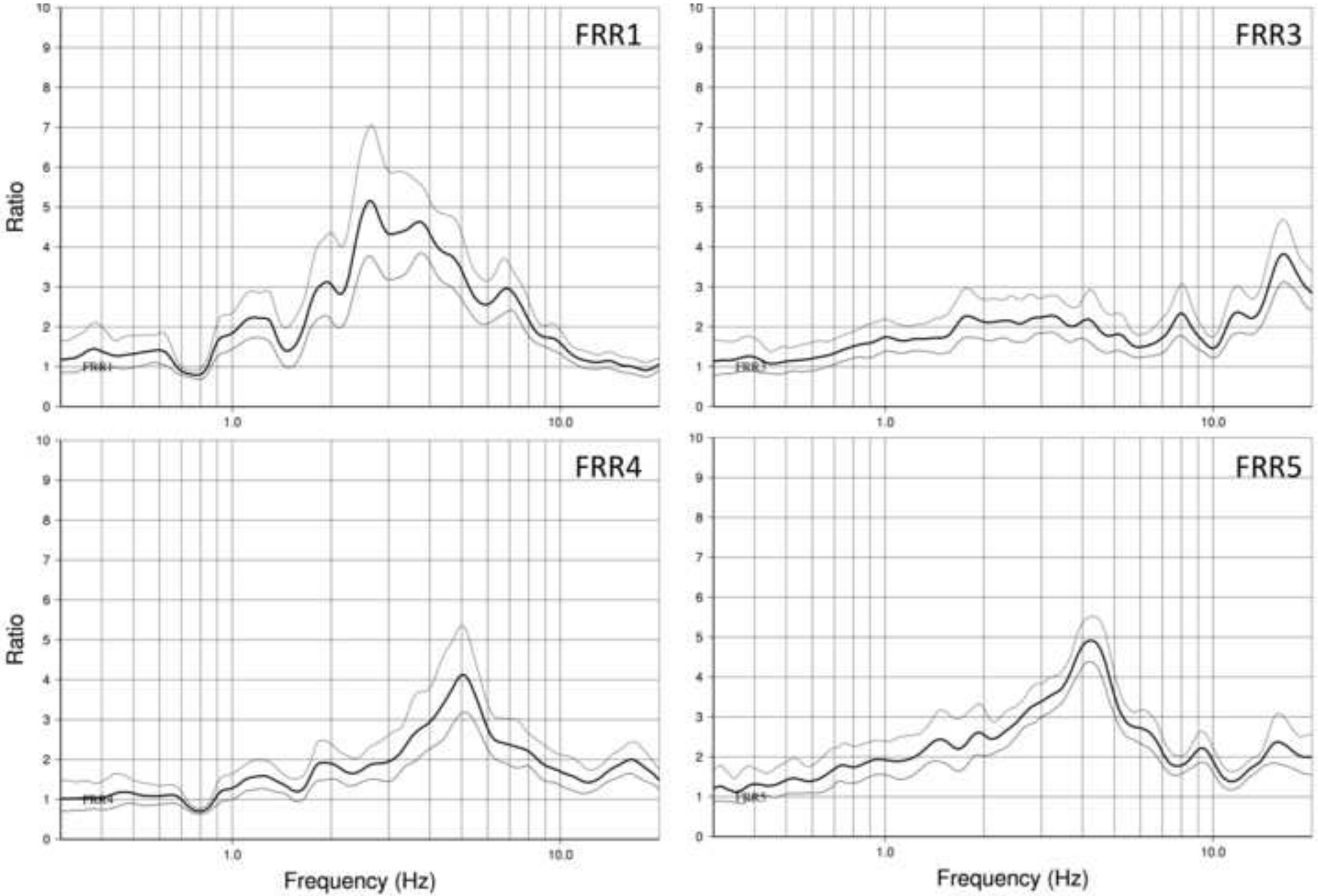

figure 7

Click here to download high resolution image

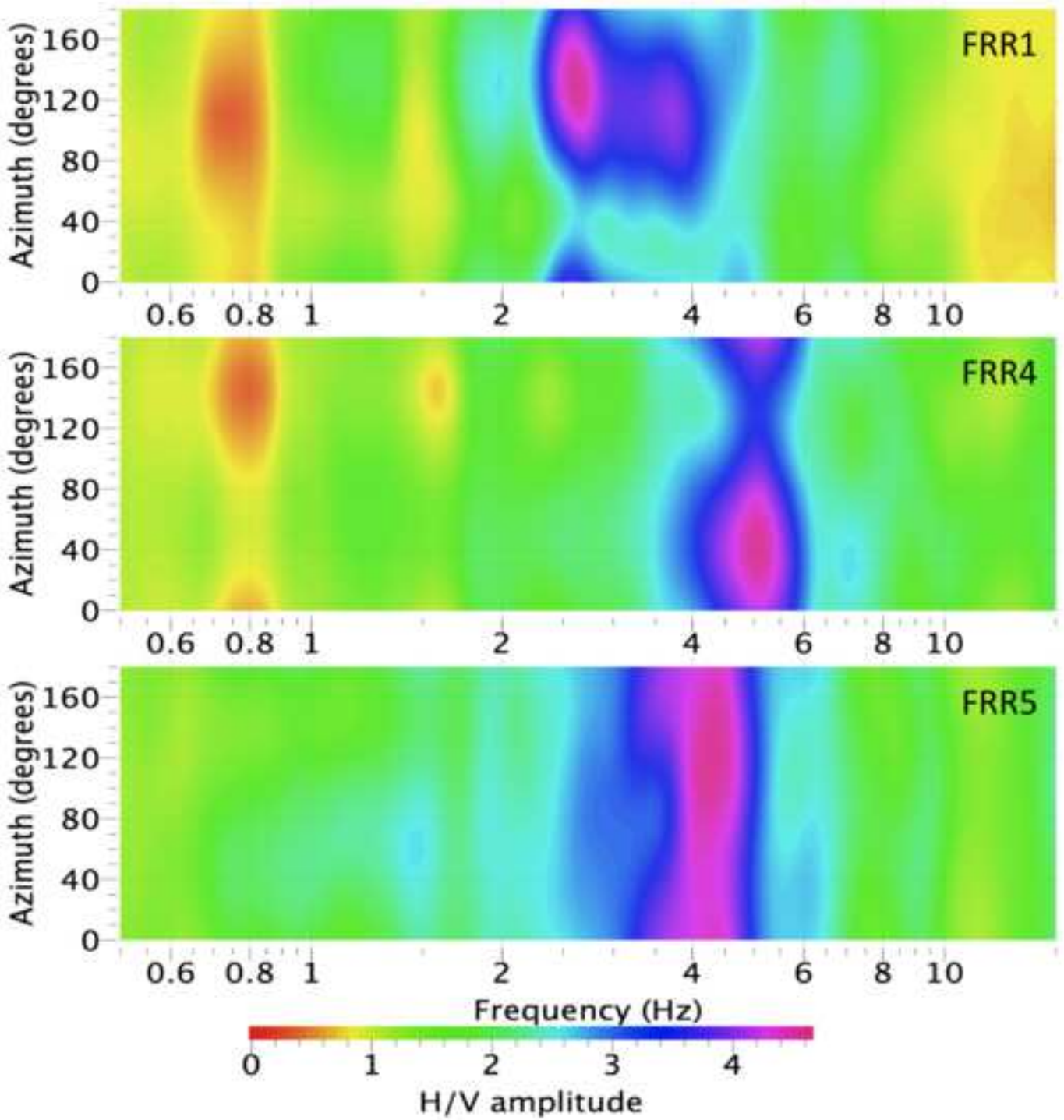

figure 8

Click here to download high resolution image

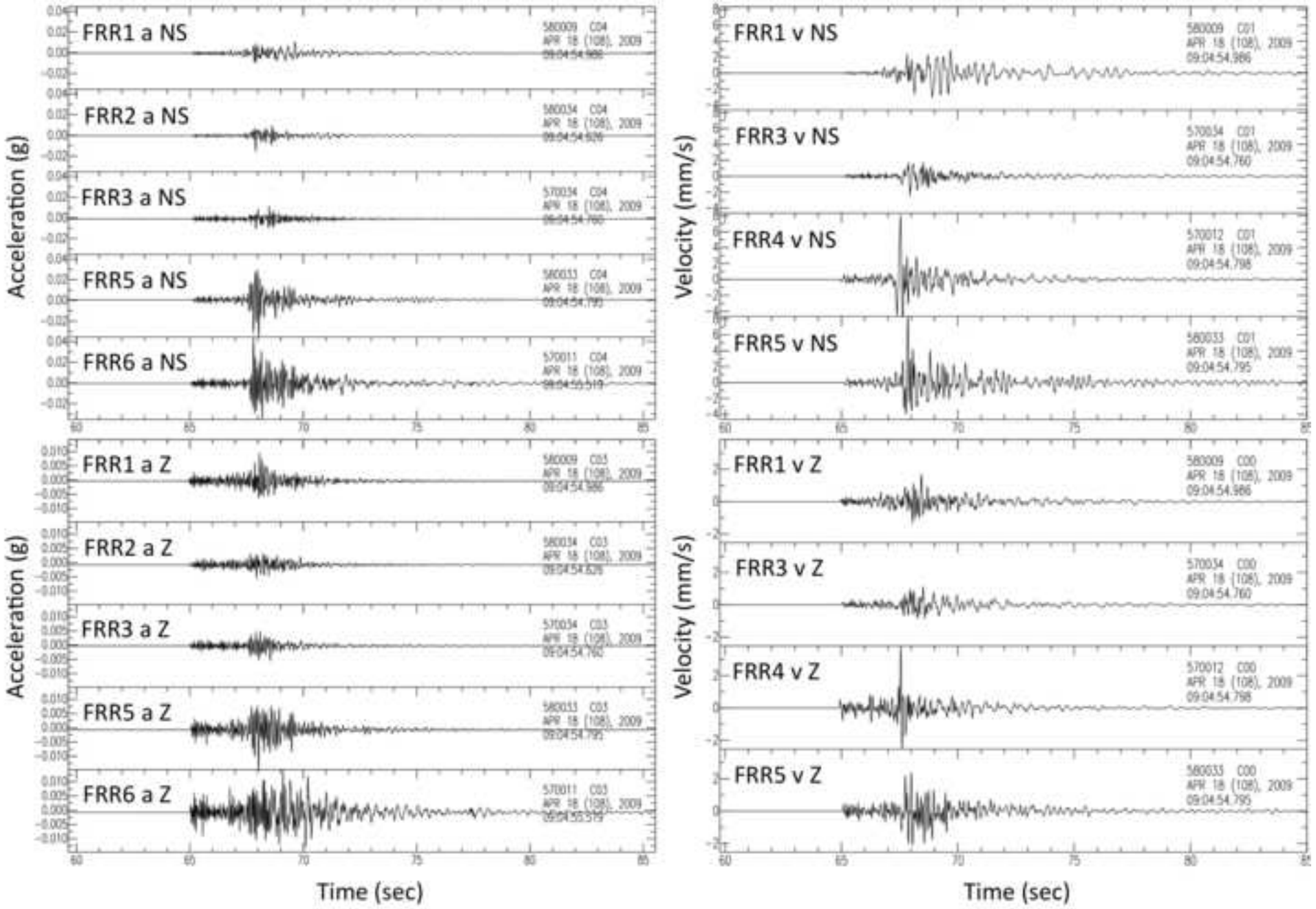

figure 9

Click here to download high resolution image

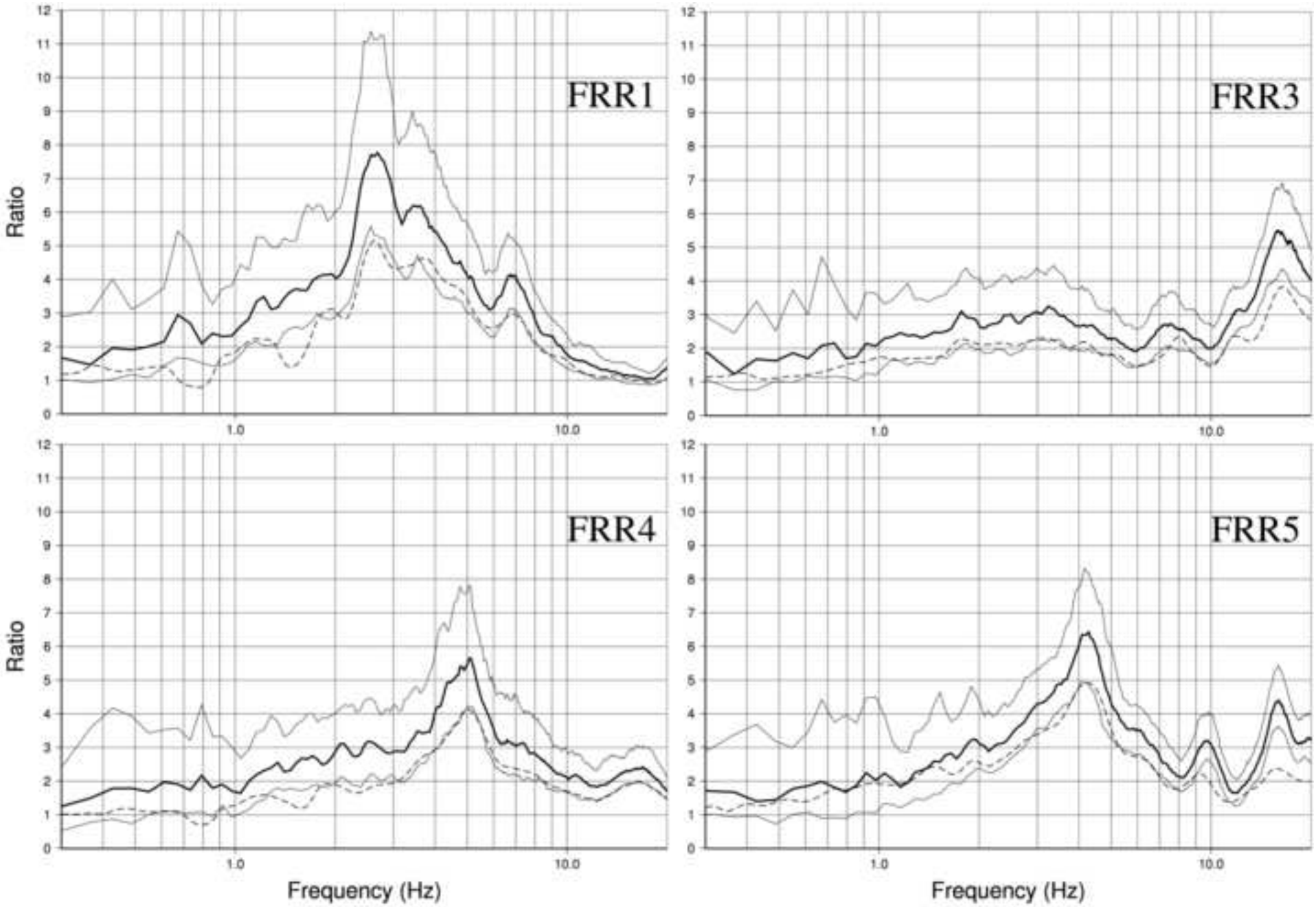

figure 10

Click here to download high resolution image

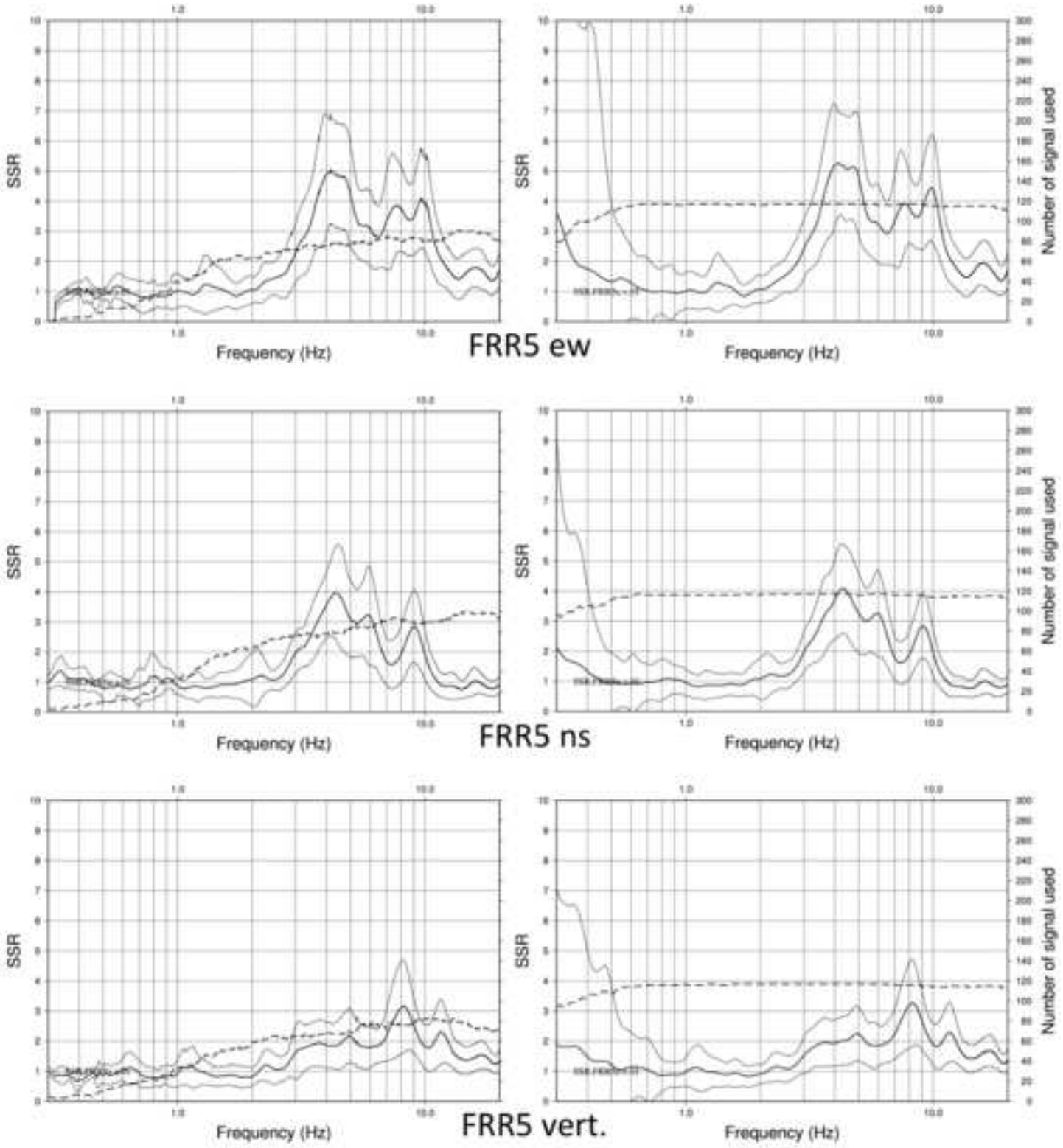

figure 11

Click here to download high resolution image

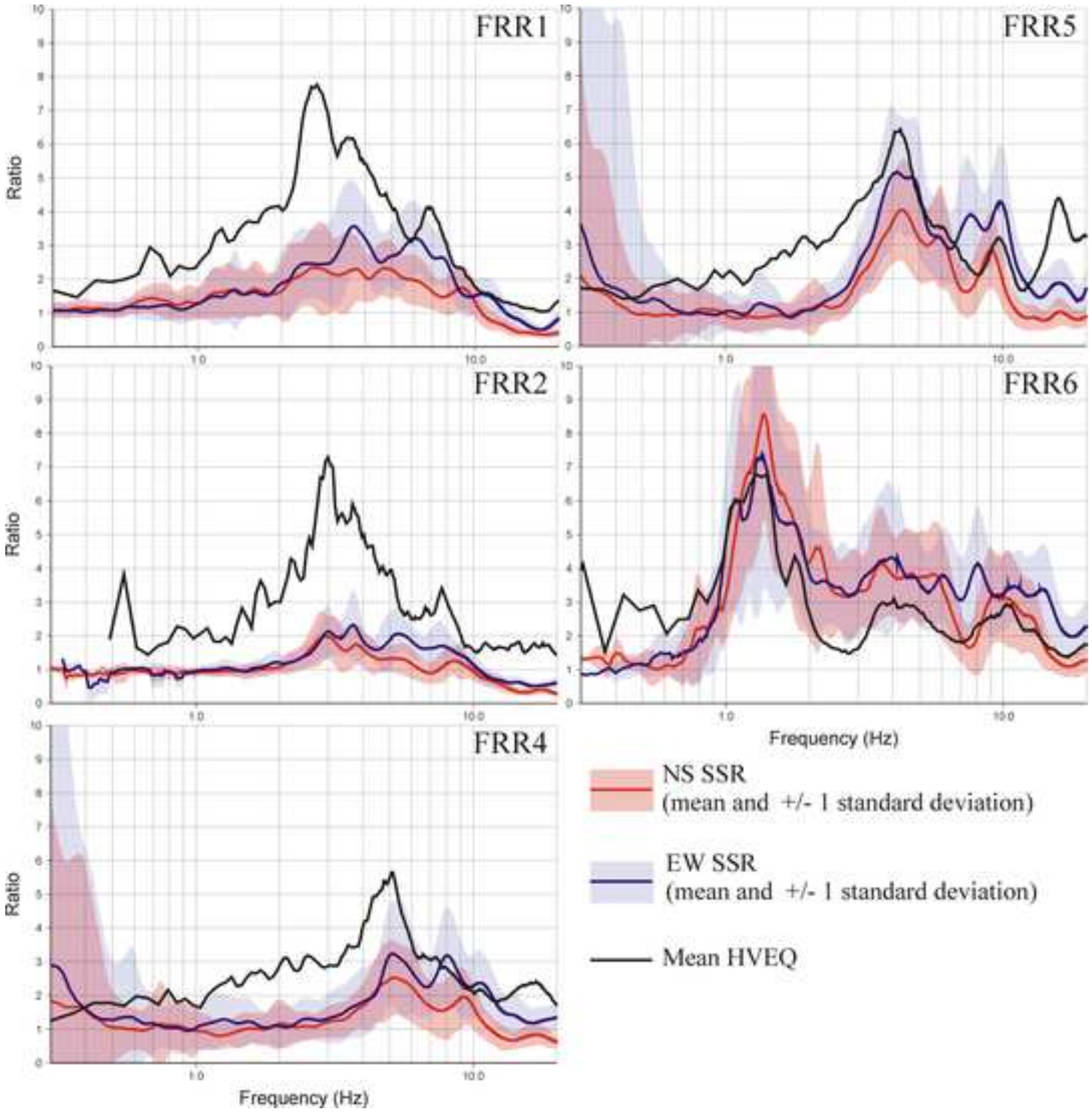

figure 12

Click here to download high resolution image

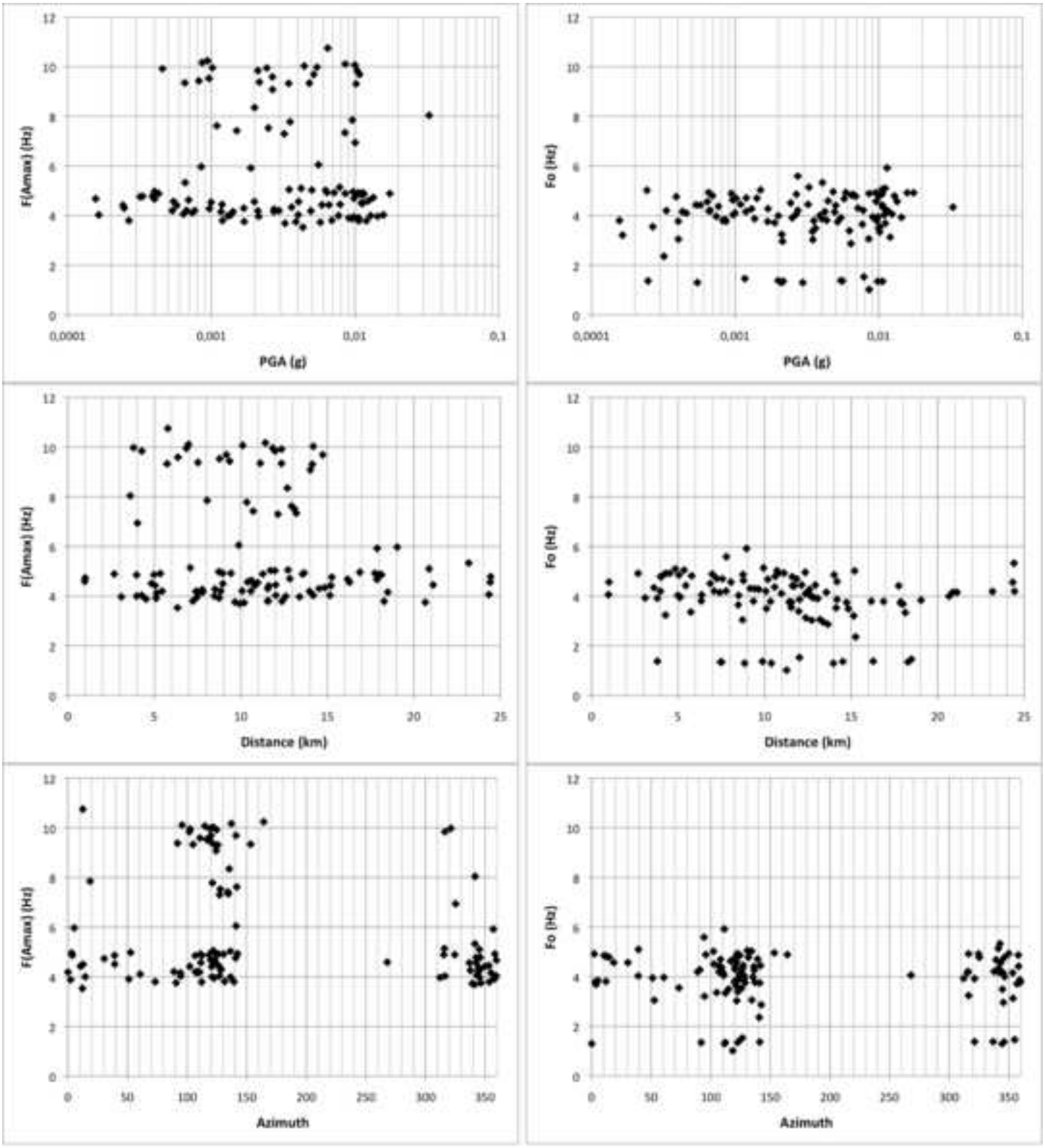

figure 13
Click here to download high resolution image

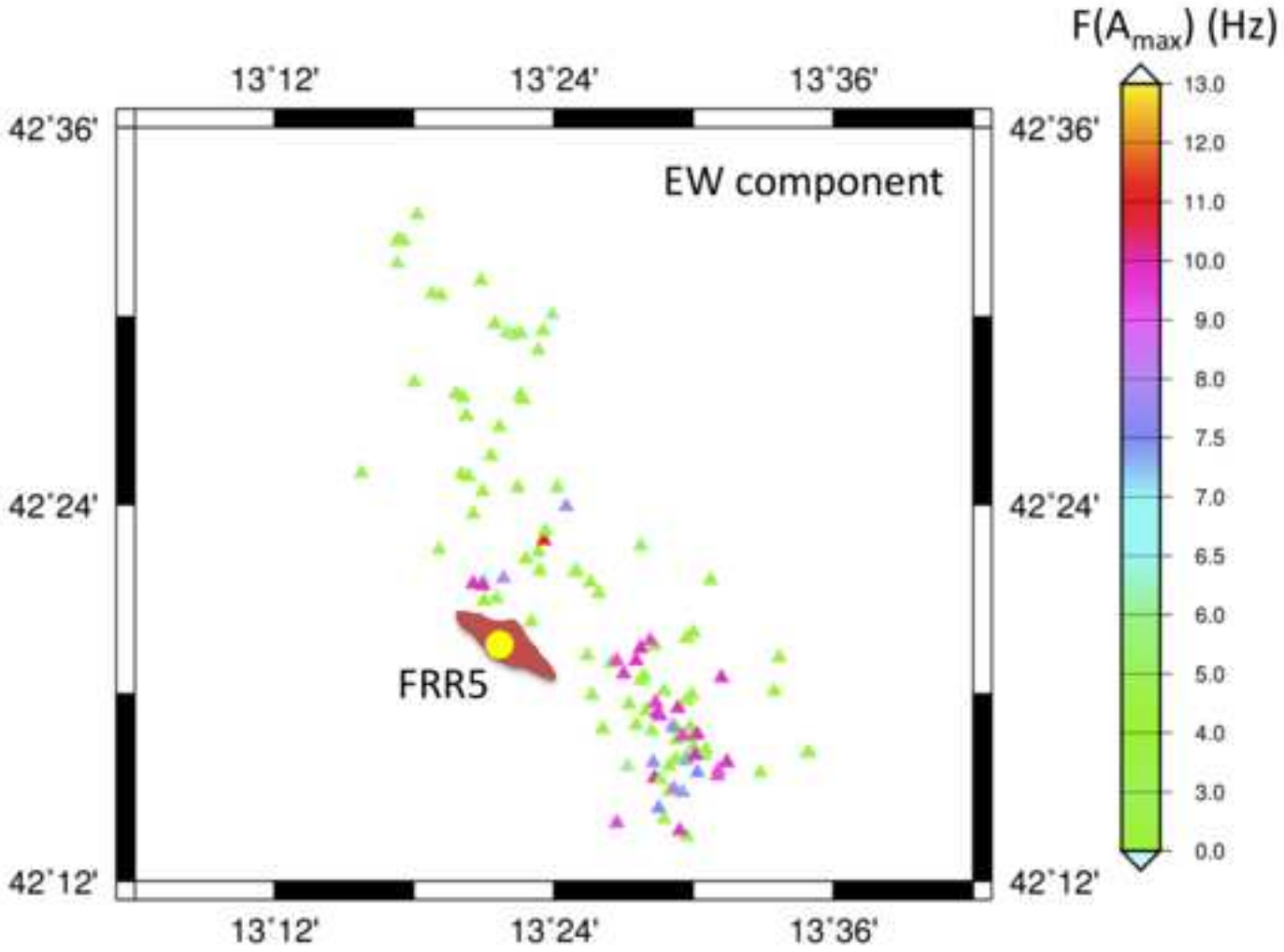

figure 14

Click here to download high resolution image